# Allosteric model of an ion pump

Eiro Muneyuki[1,*] and Ken Sekimoto[2,3]

[1]*Faculty of Science and Engineering, Department of Physics, Chuo University, Kasuga, Bunkyo-ku, Tokyo 112-8551, Japan*
[2]*MSC CNRS/UMR 7057, Université Paris 7, 10 rue Alice Domon et Léonie Duquet, 75205 Paris 13, France*
[3]*Gulliver CNRS/UMR 7083, ESCPI, 10 ru Vauquelin, F75231 Paris Cedex 05, France*

We present a simple model of a free-energy transducer made of allosterically coupled two ratchet subsystems. Each of the subsystems transports particles from one particle reservoir to another. The coupling of the subsystems imposes correlated transitions of the potential profiles of the two subsystems. As a result, a downhill flux in one subsystem with higher chemical-potential difference drives an uphill flux in the other subsystem with lower chemical-potential difference. The direction of the driven flux inverts depending on the direction of the driving flux. The ratio between the fluxes conveyed by the two subsystems is variable and nonstoichiometric. By selecting appropriate parameters, the maximum ratio of the driven flux to driving flux and maximum free-energy transducing efficiency reaches some 90 and 40%, respectively. At a stalled state, the driven flux vanishes while the driving flux remains finite. The allosteric model enables explicit analysis of the timing between binding-unbinding of particles and transitions of potential profile. The behavior of the model is similar to but different from that of the alternate access model, which is a biochemical model for active transport proteins. Our model works also as a regulatory system. We suggest that the correlated transitions of the subsystems (subunits or domains) through allosteric interaction are the origin of the diverse functions of the protein machineries.

PACS number(s): 05.40.−a, 82.37.−j, 87.16.Uv, 87.15.A−

## I. INTRODUCTION

The studies of biological molecular machines urged the development of thermal ratchet model [1–10], and it has been applied to actual ion pumps [11–16] and motor proteins [8,17–19]. The main interest in the ratchet model was to induce an active transport through the off-equilibrium change of potential-energy profiles for the transported object. In real molecular machines, it is allosteric conformational changes that change the potential-energy profiles. A driving system, such as adenosine triphosphate (ATP) hydrolysis cycle or transmembrane ionic current induces those allosteric conformational changes. In the present study, we show a model for the ion pump.

The model construction principle is simple: we couple two ratchet subsystems so that their potential-energy profiles are strongly correlated. When one ratchet subsystem works as a passive channel, the passive flux causes the change of the potential profile of this subsystem. The coupling to the second ratchet system causes the change of the potential profiles of the latter subsystem. This change in turn causes the active transport by the second ratchet subsystem. Figures 1(A) and 1(B) schematize this idea. The resulting model has eight states and is very similar to the *alternate access model* proposed by biologists [20,21].

This paper is organized as follows. In Sec. II we describe the basic assumptions of our model and present mathematical formulation to analyze it. We draw attention to the symmetry of the model. In Sec. III we describe the behavior of the model: in particular we will see that the direction of

active transport can be inverted not only by the inversion of the passive flux but also by the mere change of intrinsic time constant of the allosteric transition. Sec. IV is the discussion of the results. The biological implications of our model are also discussed.

## II. MODEL

Two ratchet subsystems [Fig. 1(A)] are coupled via correlated transitions [Fig. 1(B)]. These subsystems may concern to different subunits or domains of a transport protein in biological membranes. On the left ($L$) and right ($R$) sides of each subsystem are particle reservoirs [Fig. 1(A)]. We denote by $[X_{I,L}]$ and $[X_{I,R}]$, respectively, the concentrations of particles in the left and right reservoirs of subsystem I. Likewise, we denote by $[X_{II,L}]$ and $[X_{II,R}]$ their counterparts for subsystem II. Two transports $X_{I,L} \leftrightarrow X_{I,R}$ and $X_{II,L} \leftrightarrow X_{II,R}$ occur, respectively, through the subsystem I or the subsystem II. The transport from the left reservoir to the right reservoir will be referred to as forward transport.

In the following, we will describe our model in detail together with the accompanying assumptions. We will introduce the *reduced* probability of the system to discuss the steady state and associated fluxes.

### A. System and its states

We assume that each subsystem can have two switchable potential profiles around unique particle binding site [Fig. 1(A)]. We require that, at a time, at most one particle can be bound to the binding site. We use a Boolean variables $x_I$ (for subsystem I) and $x_{II}$ (for subsystem II) to describe the occupancy of the binding sites: for example, $x_I=1$ implies that the binding site of the subsystem I is occupied. Or, $x_{II}=0$ means

───────────
*Author to whom correspondence should be addressed. FAX: +81 3 3817 1792; emuneyuk@phys.chuo-u.ac.jp
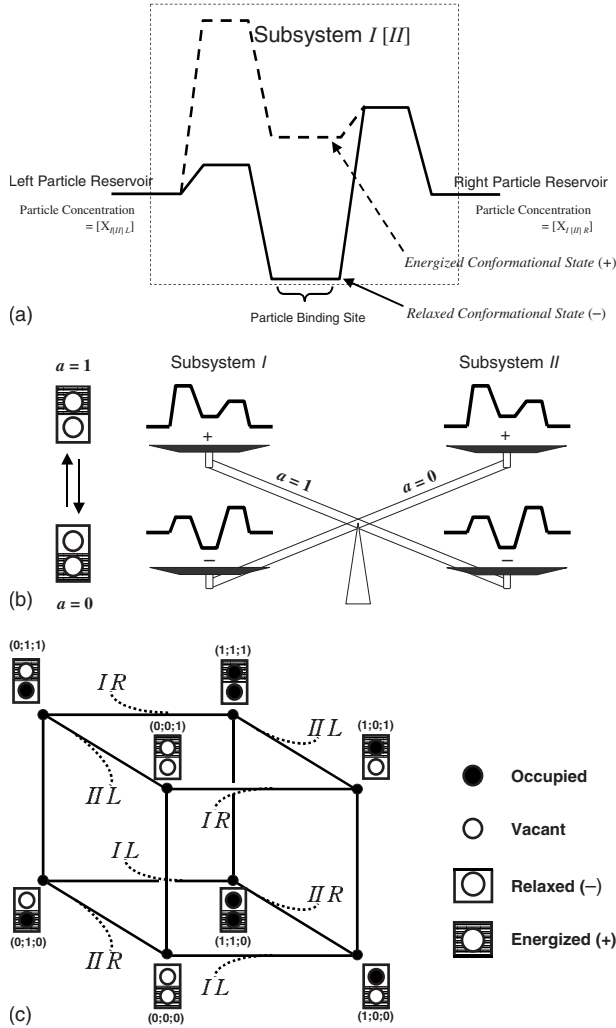
FIG. 1. (A) The potential profiles of the subsystem which sche-matically represent the energetic and kinetic parameters adopted in the model. The central well of the potential profile represents the particle binding site. Solid line indicates the potential profile of the *relaxed conformational state* (−). Broken line indicates the potential profile around the site B in its *energized conformational state* (+). (B) Allowed conformational states. Through an allosteric coupling, the two conformational states, $a=0$ (I_II$_+$) or $a=1$ (I$_+$II$_-$), are realized in a seesawlike manner. (C) The topology of the allowed transitions among the eight reduced states. The vertexes and edges correspond, respectively, to the reduced states $(x_I;x_{II};a)$ and the allowed transitions among these states. The reduced state at each vertex is represented by the Boolean indexes as well as by the symbols, where the upper [lower] squares represent subsystem I [II], respectively. The indices such as I$R$ or II$L$ attached to the dashed curves from edges indicate which subsystem exchanges a particle and with which reservoir the particle is predominantly exchanged.

that the binding site of the subsystem II is vacant. The two potential profiles are called the *energized conformational state* (+) and the *relaxed conformational state* (−). The essential assumption of our model is that the conformational states of the subsystems I and II are tightly correlated [Fig. 1(B)]: we introduce another Boolean variable $a$ to distin-guish the two coupled conformational states of the sub-

systems: when $a=0$ the subsystem I is in the state (−) and subsystem II is in the state (+) (When convenient, we will denote this state also as I_II$_+$). Inversely, $a=1$ denotes the subsystem I in the state (+) and subsystem II in the state (−) (*ibid.* as I$_+$II$_-$). While we admit the allosteric transition be-tween I_II$_+$ and I$_+$II$_-$, we exclude the combinations I_II$_-$ or I$_+$II$_+$. In Sec. III B we will relax this constraint.

The states of the whole system can then be represented by the three Boolean variables introduced above, $(x_I;x_{II};a)$, to-gether with the number of particles $n_\alpha$ in the $\alpha$th reservoirs. The first set of three variables $(x_I;x_{II};a)$ defines the *reduced state of the pump*. There are $2^3=8$ reduced states, corre-sponding to the three Boolean variables, $(x_I;x_{II};a)$. Figure 1(C) summarizes the topology of these reduced states. The indices such as I$R$ or II$L$ attached to the dashed curves indi-cate which reservoir exchanges most probably a particle with a subsystem. For example, the dashed curve with I$R$ from the reduced state $(1;1;1)$ to $(0;1;1)$ indicates that, upon the tran-sition $(1;1;1)\leftrightarrow(0;1;1)$, the migration of a particle of the species I is more likely to occur with its right reservoir. Note that in our model the allosteric transition is not tightly coupled to the displacements of particles. This feature, which is shared by another model of autonomous free-energy trans-ducer [22], is in contrast with the classical models of allos-teric transitions in which ligand binding and conformational change of a protein are tightly coupled [23].

### B. Assignment of transition rates

Our approach is the standard one [24–26]: we will indi-cate by $i$ or $j$ the state of the whole system (i.e., the system plus the particle reservoirs), which are specified by the above-defined $(x_I;x_{II};a)$ and the independent numbers $\{n_\alpha\}$ of particles in the reservoirs, such as $n_{IL}$ and $n_{IIL}$. We then define the transition rate $w_{i\rightarrow j}$ such that, during the infinitesi-mal time lapse, $dt$, the probability $P_i$ to find the whole sys-tem in the state $i$ decreases by $P_i w_{i\rightarrow j} dt$ due to this transition to the state $j$. We assume the relation of the detailed balance between a state transition $i\rightarrow j$ and its reverse $j\rightarrow i$,

$$w_{i\rightarrow j} = w_{j\rightarrow i} \exp\left(-\frac{E_j - E_i}{k_B T}\right), \qquad (1)$$

where $T$ is the temperature and $E_i$ and $E_j$ are the Gibbs free energies of the whole system at the states indicated. The transition rate $w_{i\rightarrow j}$ is then written as

$$w_{i\rightarrow j} = \frac{1}{\tau_0} \exp\left(-\frac{\Delta_{i,j} - E_i}{k_B T}\right), \qquad (2)$$

where $\tau_0$ is a global time constant and $\Delta_{i,j}(=\Delta_{j,i})$ is the height of the "saddle" point between the states $i$ and $j$. The Gibbs energy $E_i$ may have the form of $(U_i + \Sigma_\alpha \mu_\alpha n_{\alpha i})$, consisting of the free energy of the (main) system $U_i$ and the Gibbs free energy of the reservoirs, $\Sigma_\alpha \mu_\alpha n_{\alpha,i}$, where $\mu_\alpha$ is the chemical potential of the reservoir with the index $\alpha$ running over res-ervoirs, I$L$, I$R$, II$L$, and II$R$. Once we obtain the concrete expressions for the activation barriers $(\Delta_{i,j} - E_i)$, we extend them to use under nonequilibrium conditions, i.e., $\mu_{I,L} \neq \mu_{I,R}$ and/or $\mu_{II,L} \neq \mu_{II,R}$. Note that the concentrations

of particles $[X_{I,L}]$ and $[X_{II,R}]$ etc. appear only through the chemical potentials. The free energy of the system ($U_i$) is simply assumed to be the sum of the energies of the bound particles in the subsystems I and II, which we denote by $\varepsilon_I(a)$ and $\varepsilon_{II}(a)$, respectively. These energies depend on the conformational state through the variable, $a$. The subsystem(s) binding no particles, therefore, do not contribute to $U_i$.

The following three examples will tell how $E_j - E_i$ is calculated upon the transition $i \rightarrow j$. When a particle comes into the binding site of the subsystem I from the left reservoir (chemical potential: $\mu_{I,L}$), we assign $E_j - E_i = \varepsilon_I(a) - \mu_{I,L}$. When a particle in the subsystem II leaves from the binding site to the right reservoir, we assign $E_j - E_i = -\varepsilon_{II}(a) + \mu_{II,R}$. A conformational transition from $a = 0$ ($I_-II_+$) to 1 ($I_+II_-$) accompanies the change, $E_j - E_i = x_I[\varepsilon_I(1) - \varepsilon_I(0)] + x_{II}[\varepsilon_{II}(1) - \varepsilon_{II}(0)]$.

We further introduce a simplifying assumption on the energy at the binding sites,

$$\varepsilon_I(1) = \varepsilon_{II}(0), \varepsilon_I(0) = \varepsilon_{II}(1), \tag{3}$$

therefore, $\varepsilon_I(1) + \varepsilon_{II}(1) = \varepsilon_I(0) = \varepsilon_{II}(0)$. We will call [Eq. (3) and Fig. 1(B)] the "seesawlike" symmetry. Due to this symmetry, the transition back and forth between $a = 0$ and 1 are equally frequent when the binding sites are both occupied or both vacant.

### C. Probabilities and probability fluxes at the steady state

We shall denote by $i'$ the reduced state $(x_I; x_{II}; a)$ when the state of the whole system is $i$. When $i' = j'$ the two states $i$ and $j$ of the whole system differ with each other only by the numbers of particles in the reservoirs. We denote by $p'_{i'}$ the probability of the reduced state $i'$ and by $J'_{i' \rightarrow j'} (= -J'_{j' \rightarrow i'})$ the reduced probability flux, being the net probability flux from a reduced state $i'$ to another reduced state $j'$. In binding a particle from the reservoirs, the transition rate depends on the density rather than the number of the particles in the reservoirs. Therefore, while the macroscopic concentrations of the particles in the reservoirs remain quasiconstant, the transition rate $w_{i \rightarrow j}$ defined in Eq. (2) depends simply on the reduced states, or the variables $(x_I; x_{II}; a)$. We can therefore identify $w_{i' \rightarrow j'}$ with $w_{i \rightarrow j}$. Then the reduced probability flux writes in terms of the transition rate, $w_{i \rightarrow j}$ etc and the reduced probabilities,

$$J'_{i' \rightarrow j'} = -J'_{j' \rightarrow i'} = p'_{i'} w_{i \rightarrow j} - p'_{j'} w_{j \rightarrow i}. \tag{4}$$

The stationary state of the reduced description is defined by the vanishing of the sum of reduced fluxes at each reduced state, $i'$, that is, $\sum_{j'}^{(all)} J'_{j' \rightarrow i'} = 0$ for all $i'$. Here the sum is taken for all the reduced states. These conditions supplemented by the normalization condition, $\sum_{i'}^{(all)} p'_{i'} = 1$, determine all the reduced probabilities and their fluxes in the steady state. We have used the MATHEMATICA® to solve these coupled linear equations. Since the symbolic treatment of the inversion of $8 \times 8$ matrix generates too many terms, we did the calculation only numerically.

### D. Steady state particle fluxes

We denote by $\Pi^K_{L \rightarrow R}$ the net *particle* flux through the subsystem $K$ ($K = $I or II) from its left reservoir ($L$) to its right reservoir ($R$). This net *particle* flux can be related to the reduced *probability* fluxes in different ways. We will choose the following definition:

$$\Pi^K_{L \rightarrow R} \equiv \sum_{i' \rightarrow j'}^{(L \rightarrow R)} J'_{i' \rightarrow j'}. \tag{5}$$

"$L \rightarrow R$" on top of the summation signs in Eq. (5) indicates to sum over all those transitions, $i' \rightarrow j'$, through which one particle in the left reservoir is bound to the binding site of the subsystem $K$ during the transition. Upon such transition the number of the particle in the left reservoir of the subsystem $K$, i.e., $n_{K\,L}$ should undergo the change, $n_{K\,L,i} \rightarrow n_{K\,L,i} - 1 = n_{K\,L,j}$, where $i \rightarrow j$ corresponds to $i' \rightarrow j'$ in the reduced representation.

### E. Symmetry of the model

We summarize the symmetries built in our model. Firstly the model lacks the left-right symmetry ($L$ vs $R$), which is an ingredient that enables the directional transport. On the other hand we assumed that the ratchet subsystems I and II are identical and interchangeable; The net particle fluxes $\Pi^I_{L \rightarrow R}$ and $\Pi^{II}_{L \rightarrow R}$ in these subsystems are interchanged if we exchange the pair of the chemical potentials $(\mu_{I,L}, \mu_{I,R})$ with the pair $(\mu_{II,L}, \mu_{II,R})$ This symmetry implies that in our model the roles of driving subsystem and driven subsystem are attributed solely by the relative magnitudes of $\Delta\mu_I \equiv \mu_{I,L} - \mu_{I,R}$ and $\Delta\mu_{II} \equiv \mu_{II,L} - \mu_{II,R}$. While this symmetry simplifies certain physical arguments, it may also exclude or disfavors some functions of more generic model. The last point is briefly discussed in comparison with an existing biological model in Sec. IV.

### F. Linear nonequilibrium relation

Near equilibrium, i.e., for infinitesimally small $\Delta\mu_I$ and $\Delta\mu_{II}$, the Onsager coefficients are defined through the following linear relationship:

$$\begin{pmatrix} \Pi^I_{L \rightarrow R} \\ \Pi^{II}_{L \rightarrow R} \end{pmatrix} = \begin{pmatrix} L_I & L' \\ L' & L_{II} \end{pmatrix} \begin{pmatrix} \Delta\mu_I \\ \Delta\mu_{II} \end{pmatrix}. \tag{6}$$

Qualitatively, the cross coupling $L'$ in Eq. (6) can give the pumping act while $L_I$ and $L_{II}$ represent the passive leak or dissipation. These Onsager coefficients give essentially the correlation functions of the equilibrium fluctuating fluxes which we denote by $\hat{\Pi}^I_{L \rightarrow R}$, etc.,

$$L_K \propto \langle (\hat{\Pi}^K_{L \rightarrow R})^2 \rangle_{eq}, \quad L' \propto \langle \hat{\Pi}^I_{L \rightarrow R} \hat{\Pi}^{II}_{L \rightarrow R} \rangle_{eq}. \tag{7}$$

Here $K = $I or II and $\langle \cdot \rangle_{eq}$ denotes the average in equilibrium, $\Delta\mu_I = \Delta\mu_{II} = 0$ (hence $\langle \hat{\Pi}^I_{L \rightarrow R} \rangle_{eq} = \langle \hat{\Pi}^{II}_{L \rightarrow R} \rangle_{eq} = 0$). We should

TABLE I. The parameters for the potential profiles. The suffixes to indicate subsystem I and II are omitted in the table because the potential profiles are the same for the two subsystems. $\tau_0$ is the global time constant in Eq. (2). $\mu_L^0$ and $\mu_R^0$ are the standard chemical potential of the transported particle in the left and right reservoirs. The chemical potential is related to the standard chemical potential as follows: $\mu_{L[R]} = \mu_{L[R]}^0 + k_B T \ln[X]_{L[R]}$, where the $[X]_{L[R]}$ are the macroscopic concentration of the particles in the left [right] reservoirs. $\Delta_L$ and $\Delta_R$ are the height of the "saddle point" associated to the binding and unbinding of a particle to the left or right reservoir, respectively. $\Delta_{x_I,x_{II}}^{AT}$ denotes the height of the "saddle point" for allosteric transition with an occupancy state $(x_I, x_{II})$. The parameters $\varepsilon$ are the energies attributed to a particle on the binding site in Eq. (3). In order to fix the parameter values, we first arbitrarily fixed the global time constant ($\tau_0$) as $10^{-11}$ s, $\Delta_{0,0}^{AT}$ as 6 $k_B T \ln 10$ and $\mu_L^0$ and $\mu_R^0$ as 0. Then, we searched for the values of $\Delta_L$, $\Delta_R$, $\Delta_{x_I,x_{II}}^{AT}$, and $\varepsilon$ which achieve high coupling ratio under the given concentrations $([X_{I,L}], [X_{I,R}], [X_{II,L}], [X_{II,R}]) = (1, 0.01, 1, 1)$ and under a given "total time" of the allosteric transitions defined as $1/w_{(x_I,x_{II},0) \to (x_I,x_{II},1)}$ $+ 1/w_{(x_I,x_{II},1) \to (x_I,x_{II},0)} = 2 \times 10^{-5}$ s. Those values in the table is what we found within the following ranges: $k_B T \ln 10 \leq \Delta_{L[R]} - \mu_{L[R]}^0$ $\leq 6$ $k_B T \ln 10$, $k_B T \ln 10 \leq \Delta_{L[R]} - \varepsilon \leq 6$ $k_B T \ln 10$. Apart from these basic setting, we fixed all $\Delta_{x_I,x_{II}}^{AT}$'s to be 6 $k_B T \ln 10$ in Fig. 3, for simplicity. Also in Fig. 5, we added $\delta^{AT}$ to $\Delta_{x_I,x_{II}}^{AT}$ to change the characteristic time of the allosteric transitions.

| | Relaxed state | Energized state |
|---|---|---|
| $\tau_0$ | $10^{-11}$ | |
| $\mu_L^0$ | 0 | 0 |
| $\Delta_L$ | 8 $k_B T \ln 10$ | 13 $k_B T \ln 10$ |
| $\varepsilon$ | $-3$ $k_B T \ln 10$ | 2 $k_B T \ln 10$ |
| $\Delta_R$ | 10 $k_B T \ln 10$ | 10 $k_B T \ln 10$ |
| $\mu_R^0$ | 0 | 0 |
| $\Delta_{0,0}^{AT}$ | 6 $k_B T \ln 10$ | |
| $\Delta_{0,1}^{AT}$ | 6 $k_B T \ln 10$-$k_B T \ln 500$ | |
| $\Delta_{1,0}^{AT}$ | 6 $k_B T \ln 10$-$k_B T \ln 500$ | |
| $\Delta_{1,1}^{AT}$ | 5 $k_B T \ln 10$ | |

*not* expect generally $L_I = L_{II}$ because the Onsager coefficients depend on $[X_I]$ or $[X_{II}]$ and, therefore, on $\mu_I$ or $\mu_{II}$ See Sec. III C for one of the consequence of this fact.

## III. RESULTS

### A. Direction of the particle fluxes and the *coupling ratio*

In order to identify the directions of the active particle transport, we imposed nonequilibrium among the reservoirs of the subsystem I ($\mu_{I,L} \neq \mu_{I,R}$ or $[X_{I,L}] \neq [X_{I,R}]$) while keeping in equilibrium among the reservoirs of the subsystem II; ($\mu_{II,L} = \mu_{II,R}$ or $[X_{II,L}] = [X_{II,R}]$). With the values of parameters given in Table I, we found that a rightward particle flux in subsystem I induces a leftward particle flux in subsystem II, and vice versa (Fig. 2).

We shall call *driving subsystem* the subsystem whose two reservoirs have larger chemical-potential difference than the other subsystem. The latter subsystem is called *driven subsystem*. The coupling of the fluxes is characterized by the
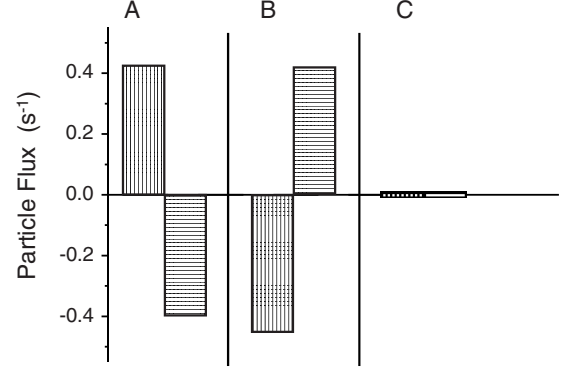


FIG. 2. Examples of the coupled particle fluxes in the subsystem I ($\Pi_{L \to R}^I$: vertically striped bars) and in the subsystem II ($\Pi_{L \to R}^{II}$: horizontally striped bars). The concentration in the reservoirs ($[X_{I,L}]$ $[X_{I,R}]$; $[X_{II,L}]$, and $[X_{II,R}]$) are (1, 0.01; 1, 1) in (A), (0.01, 1; 1, 1) in (B), and (1, 1; 0.01, 0.01), i.e. equilibrium, in (C).

*coupling ratio q*,

$$q = -\frac{(\text{particle flux})_{Driven\ subsystem}}{(\text{particle flux})_{Driving\ subsystem}}, \quad (8)$$

where the minus sign in Eq. (8) was introduced to render the ratio $q$ positive. Near the equilibrium, in particular, this ratio is given by the Eqs. (6) and (7),

$$q \approx -\frac{L'}{L_I} = -\frac{\langle \hat{\Pi}_{L \to R}^I \hat{\Pi}_{L \to R}^{II} \rangle_{eq}}{\langle (\hat{\Pi}_{L \to R}^I)^2 \rangle_{eq}} (\text{near equilibrium}) \quad (9)$$

Here again, the minus sign was introduced to render the ratio $q$ positive.

Two remarks are in order: first we can identify $q$ by $-L'/L_I$ only *in the linear regime*. In general the magnigude of $q$ should change if we change the sign of $\Delta\mu_I$ (or that of $\log([X_{I,L}]/[X_{I,R}])$) due to the lack of left-right symmetry in the model. In other words, the difference of the values of $q$ upon the exchange of the sign of $\Delta\mu_I$ gives a measure of how far the system is from equilibrium. For example, the concentration gradient of $([X_{I,L}], [X_{I,R}]) = (1, 0.01)$ yielded $q = 93.51\%$, while for the gradient of $([X_{I,L}], [X_{I,R}])$ $= (0.01, 1)$ yielded $q = 93.49\%$. Secondly, it is evident that the coupling ratio is not a stoichiometric number. In this sense the present model is a *loose-coupling* model.

Within the framework of linear nonequilibrium thermodynamics, it is not surprising that the change of the sign of $\Delta\mu_I$ changes the sign of the driven particle flux, $\Pi_{L \to R}^{II} = L' \Delta\mu_I$. Intuitively, however, it might not be evident how a single allosteric degree of freedom can control the direction of active transport. A key is that the variation of $a(t)$ is not a predetermined function of time, but a part of system's response. We will discuss this point in Sec. IV A.

### B. Effect of the looseness of the allosteric coupling

Only in this subsection we relax the coupling condition of the potential profiles of the two ratchet subsystems: we allow also the states I$_+$II$_+$ and I$_-$II$_-$ in addition to I$_-$II$_+$ ($a = 0$) and
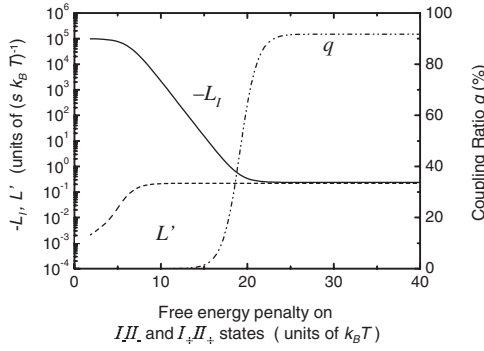
FIG. 3. Effect of the looseness of the allosteric coupling on the individual particle fluxes and the coupling ratio. The horizontal axis shows the free-energy penalty imposed on $I_+II_+$ and $I_-II_-$ conformational states relative to $I_-II_+$ and $I_+II_-$ conformational states. The Onsager coefficients, $-L_I$ (solid line) and $L'$ (broken line), are shown. These coefficients are obtained by solving Eq. (6) at $[X_{I,L[R]}]$ and $[X_{II,L[R]}]$ near 1. The coupling ratio $q$ is also shown by dash-double dotted line. In this calculation, $\Delta^{AT}_{x_I,x_{II}}$'s are all set to be $6\ k_B T \ln 10$.

$I_+II_-$ ($a=1$) conformations. We impose an equal energetic penalty to the additional two states $I_+II_+$ and $I_-II_-$, with respect to the "seesaw" states $I_-II_+$ and $I_+II_-$. The driven flux will vanish in the absence of the penalty, while the infinitely high penalty should achieve the maximal coupling ratio. In Fig. 3, we show how this penalty affects the Onsager coefficients $-L_I$ and $L$, which corresponds, respectively, to the driving flux $\Pi^I_{L\to R}$ and the driven flux $(-\Pi^{II}_{L\to R})$ under a fixed driving chemical-potential gradient, $\Delta\mu_I$ (and $\Delta\mu_{II}=0$). We notice that these two fluxes responds differently to the energetic penalty on the states $I_+II_+$ and $I_-II_-$. In the figure the coupling ratio $q=|L'|/L_I$ is also plotted.

### C. Regulatory point of view of the driven subsystem

There is one aspect which a formal Onsager's force-flux relation does not capture. This is the dependence of the Onsager coefficients on the (average) level of chemical potentials. For example, in the situation studied above, $\Delta\mu_{II}=0$,
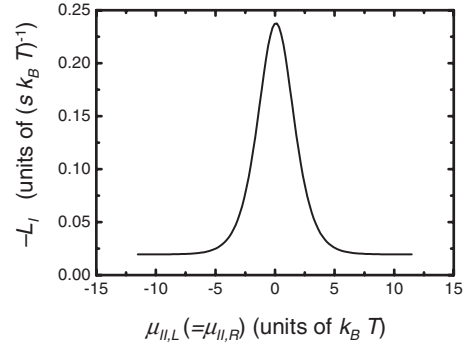


FIG. 4. Regulation effect of subsystem II on subsystem I. The Onsager coefficient $-L_I$ is plotted against $\mu_{II,L}=\mu_{II,R}$. The coefficient was determined as in Fig. 3.

the driving flux $\Pi^I_{L\to R}$ in the driving subsystem is found to depend strongly on the chemical potentials $\mu_{II,L}=\mu_{II,R}$, or, on the particle concentrations $[X_{II,L}]=[X_{II,R}]$, in the reservoirs of the subsystem II. The condition corresponds to a single reservoir for the subsystem II. See Fig. 4. At a certain concentration of the particle in subsystem II, the flux in the subsystem I is maximized by an order of magnitude. In biochemical terms, this result can be interpreted as a catalytic reaction in the subsystem I which is regulated by the concentration of the allosteric cofactor, i.e. the particle in subsystem II. Although direct mechanistic relevance is not clear, such a dual effect by a single species of ligand is observed in real biological systems [27–29]. A flux circulating between the subsystem II and its single reservoir is induced by the concentration gradient in the subsystem I simultaneously. The flux shows a bell-shaped dependency on the particle concentration of the subsystem II and this concentration correlates with $[X_{I,L}]$ and $[X_{I,R}]$ (data not shown). Viewed from another side, the subsystem II can also function as sensor of particle concentration range in the subsystem I.

The dependence of $\Pi^I_{L\to R}$ on the chemical-potential difference $\Delta\mu_I$ is also modified by $\mu_{II,L}(=\mu_{II,R})$ (data not shown).



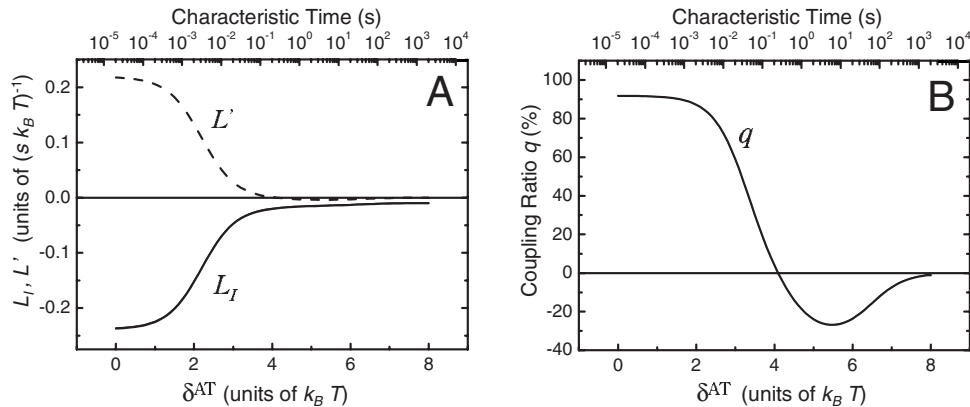FIG. 5. Effect of the characteristic time of the allosteric transitions on transport properties. $\delta^{AT}$ was added to $\Delta^{AT}_{x_I,x_{II}}$ in Table I to change the barrier height of the allosteric transitions. The characteristic time of the transitions is shown in the upper axis. (A) Onsager coefficients $L_I$ (solid line) and $L'$ (broken line) are shown. The coefficient was determined as in Fig. 3. (B) coupling ratio.

### D. Flux inversion controlled by the time constants of the allosteric transition

Our model shows an intriguing phenomenon with regard to the time constant of the allosteric transition. When the activation (free) energy barrier related to the allosteric transition ($\Delta^{AT}_{x_I, x_{II}}$, Table I) and hence the characteristic time of the allosteric transitions is changed [see Eq. (2)] by adding $\delta^{AT}$, the coupling ratio changes its sign, i.e., the subsystem II is driven in the opposite direction. Figure 5(A) shows the Onsager coefficients $L_I$ and $-L'$, which corresponds, respectively, to the driving flux $\Pi^I_{L \to R}$ and the driven flux $\Pi^{II}_{L \to R}$ in the linear regime. Figure 5(B) shows the coupling ratio $q$

against the same control parameter. While the decrease in the transport fluxes seems to be natural with the increase the time constant of allosteric transition, the direction inversion of the driven flux implies nontrivial change of the timing, or the pathway, of transport process using only a simple switching between $a = 0$ and 1. In Sec. IV A we will discuss on this point in the context of the rate-limiting steps.

### E. Free-energy transduction efficiency

When the subsystems I [II] are the driving [driven] systems, respectively, the free-energy transduction efficiency (energy efficiency for short), $\eta$, is defined as follows:

$$\eta \equiv -\frac{(\text{chemical potential difference}) \times (\text{particle flux})_{Driven\ subsystem}}{(\text{chemical potential difference}) \times (\text{particle flux})_{Driving\ subsystem}}$$

$$= -\frac{\Delta\mu_{II}\Pi^{II}_{L \to R}}{\Delta\mu_I\Pi^I_{L \to R}} \quad (\Delta\mu_I > \Delta\mu_{II}) = -\frac{\Delta\mu_I\Pi^I_{L \to R}}{\Delta\mu_{II}\Pi^{II}_{L \to R}} \quad (\Delta\mu_{II} > \Delta\mu_I). \tag{10}$$

In particular, in the linear nonequilibrium regime [Eq. (6)], the energy efficiency is represented by the Onsager coefficients and the ratio, $X \equiv \Delta\mu_{II}/\Delta\mu_I$, as $\eta = -X(L_{II}X + L')/(L_I + L'X)$ Fig. 6 shows an example of the energy efficiency as function of $\Delta\mu_I - \Delta\mu_{II} > 0$, beyond linear nonequilibrium regime. In the linear nonequilibrium regime, and where the energy efficiency $\eta$ or the driven flux $\Pi^{II}$ vanishes, the relation, $|L'|\Delta\mu_I = L_{II}\mu_{II}$, is satisfied according to [Eq. (6)].

A remark is in order here: the function of the energy efficiency vs $X(=\Delta\mu_{II}/\Delta\mu_I)$ is singular at equilibrium $\Delta\mu_{II} = \Delta\mu_I = 0$. However, this singularity has no physical significance at the microscopic level since, in the very vicinity of the equilibrium, the fluctuating fluxes in $\hat{\Pi}^I_{L \to R}$, etc., dominate over the systematic fluxes [see Eq. (7) also]. The coupling between two fluctuating fluxes at equilibrium was recently reported by Komatsu and Nakagawa in the context of the Feynman's ratchet [30].
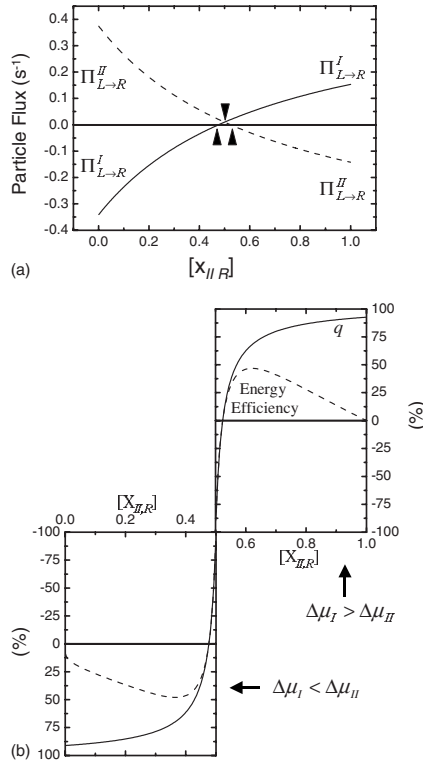


FIG. 6. (A) Individual particle flux $\Pi^I_{L \to R}$ and $\Pi^{II}_{L \to R}$ vs $[X_{II,R}]$. The other concentrations are $([X_{I,L}], [X_{I,R}], [X_{II,L}]) = (1, 0.5, 1)$. The particle flux of driving and driven subsystem is shown by solid and broken line, respectively. ▼: the points where $\Delta\mu_I$ and $\Delta\mu_{II}$ balance; ▲: the points where driven flux vanishes while the driving flux remains finite (stall state or static head). (B) coupling ratio ($q$, solid curves) and free-energy transduction Efficiency (energy efficiency, broken curves) vs $[X_{II,R}]$. The relative magnitudes of $\Delta\mu_I$ and $\Delta\mu_{II}$ are indicated within the figure.

## IV. DISCUSSION

### A. How the inversion of driven flux is realized

We first discuss how the direction of driven particle flux can be inverted by the inversion of the source flux $\Delta\mu_I$ (Fig. 2). Then we discuss the flux inversion by the change of the time constant of allosteric transition (Fig. 5).

*Inversion of driven flux by the inversion of driving flux*: if we agitate randomly a coffee spoon immersed in water, the water will be heated up by the "Joule" heat. The allosteric transition in our model occurs also randomly. But the latter random motion can decrease the entropy of the *driven* subsystem against a chemical-potential gradient. The key difference from the former case is that the allosteric transition is correlated to the state of the driven subsystem, while the
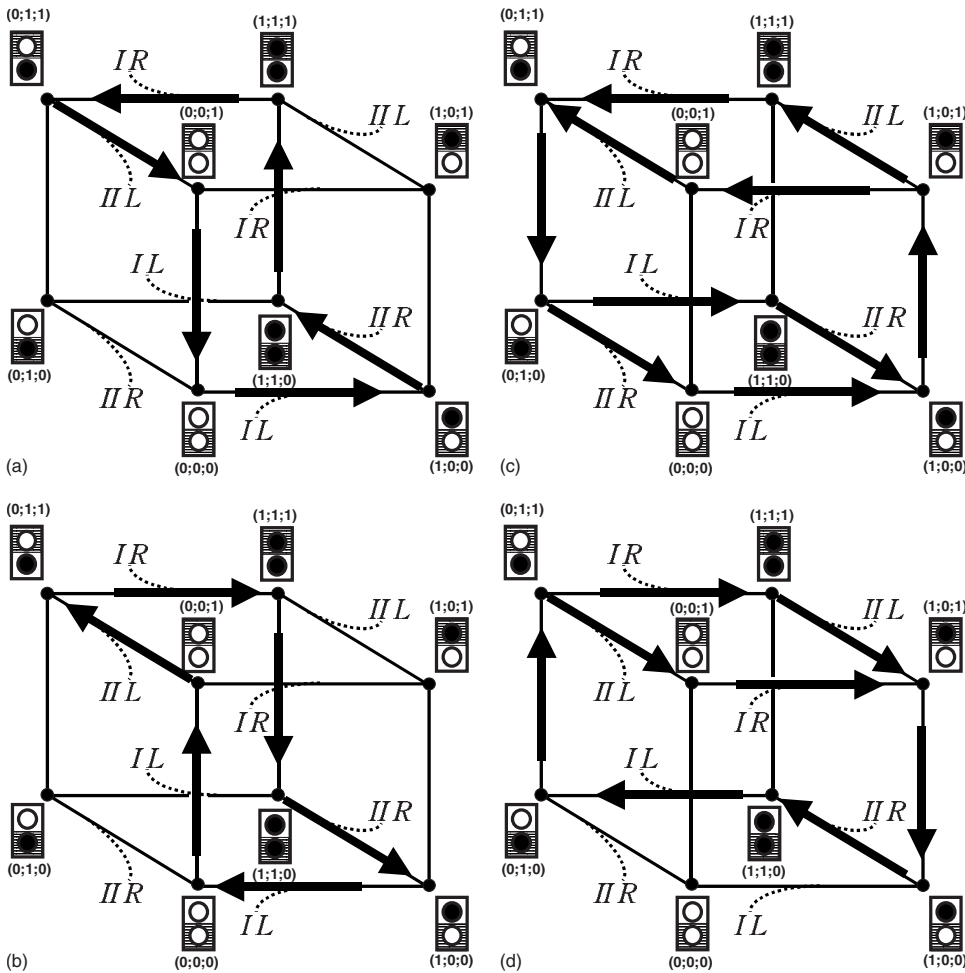
FIG. 7. The dominant pathway of coupled particle flux under the condition of Figs. 2 and 5. Eight reduced states and possible transitions are shown as in Fig. 1(C). The dominant pathway is indicated by thick arrows. (A) and (B) correspond to Figs. 2(A) and 2(B), respectively. (C) corresponds to Fig. 5 with the characteristic time of the transitions of ca. 6 s. (D) is the same as (C) except that the driving force is inverted.

spoon does not respond to the motion of water molecules. Scrutiny of the probability fluxes shows that, as far as the allosteric degree of freedom is flexible enough (i.e., with small time constant), allosteric transitions should mostly occur when both subsystems are occupied or none is occupied, that is between the reduced state $(0,0,0)$ and $(0,0,1)$ and between $(1,1,0)$ and $(1,1,1)$ on the cubic diagram of Fig. 1(C). Besides, there are the reduced states, $(1,0,0)$ and $(0,1,1)$, where the system spends most of time. The closed circuit on the cubic diagram which is representative of the process (*dominant pathway*, for short) is then found as shown in Fig. 7(A) $(\Delta\mu_I < 0)$ and Fig. 7(B) $(\Delta\mu_I > 0)$. Although the dominant pathway is unchanged for these cases, the rate-limiting steps are located at different states on this pathway: while for $\Delta\mu_I < 0$ the driving subsystem I at $(0,1,1)$ or at $(1,0,0)$ waits for a process in the driven subsystem II, the situation is inversed for $\Delta\mu_I > 0$. It is this difference that causes the inversion of particle flux.

*Inversion of driven flux through the timing control*: the increase in the time constant of allosteric transition makes the allosteric transition itself be the rate-limiting steps and, therefore, favors the local equilibration under a given conformational state $a$. It then causes the change of the dominant pathway, with allosteric transitions now occurring between $(0,1,0)$ and $(0,1,1)$ and between $(1,0,0)$ and $(1,0,1)$, see Fig. 7(C) for $\Delta\mu_I < 0$ and Fig. 7(D) for $\Delta\mu_I > 0$. Again the dominant pathway is the same for $\Delta\mu_I < 0$ and $\Delta\mu_I > 0$ except

that transition from $(1,0,0)$ to $(0,1,0)$ via $(0,0,0)$ is not prominent in the latter case. In summary the flux inversion through the time constant of the allosteric transition is associated to the change of dominant pathway.

### B. Relevance to other models and biological systems.

*Comparison with the existing Brownian ratchet models:* many attempts have been made in the context of energetics of the Brownian ratchet models. Zhou and Chen bound the chemical reaction to mechanical motion [31]. Astumian and Bier [7] considered the AT(D)P binding which invokes the shape transition of the ratchet. Parmeggiani *et al.* bound the chemical reaction to the change of transition rate of ratchet model [32]. In all these works there lacks *explicit* mechanisms of driving subsystem.

Our model is closer to the reality in this sense. Moreover, the symmetry of our model permits to study trivially the consequences when the roles of driving and driven systems are exchanged. The maximal energy transducing efficiency, being some 40% in our study, is a matter of parameter tuning [22].

*Comparison with existing biological models:* we have concretized the biochemical concept of conformational coupling for energy transduction proposed by Boyer [33] through an allosteric degree of freedom. The dominant pathway [Fig. 7(A)] of our model is represented as the schema
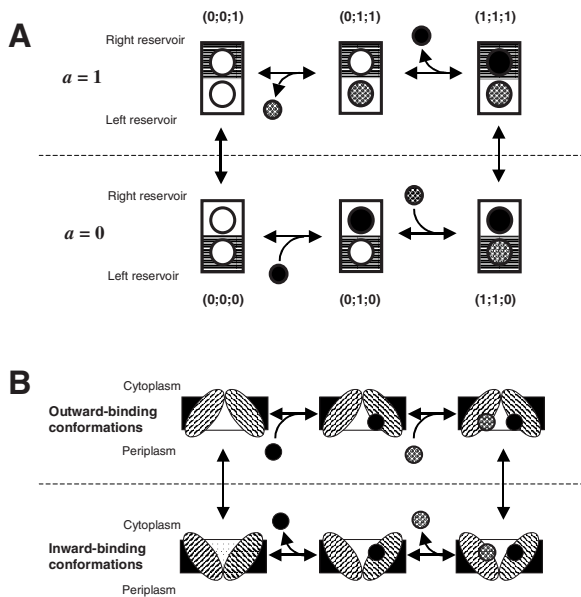
FIG. 8. Comparison of the present model with *alternate access model* for biological pumps. (A) Representation of the dominant pathway in Fig. 7(A). The meaning of the symbols is the same as Fig. 7 except that the particle transported by subsystem I and II are discerned by black circle and checkered circle. (B) Alternate access model for a symporter protein (modified from [21]). The two kinds of transported molecule are shown by black circle and checkered circle, respectively. The protein takes two conformations, outward-binding conformation and inward-binding conformation.

[Fig. 8(A)]. There is a prevailing model of transporter protein on biological membranes, called *alternate access model* [20]. This model was supported strongly from the recent

structural study of transport proteins [21] [schema Fig. 8(B)]. If we compare these schemas, we find that the transition between $I_+II_-$ and $I_-II_+$ conformational states of the system corresponds to the transition between *inward-binding* and *outward-binding* conformation of the transporter of the alternate access model. The timing of the energy state transition has also something in common; it occurs mainly when the binding sites of the two subsystems are simultaneously occupied or empty in our model [Fig. 8(A)] and both binding sites for the different solutes are occupied or empty in the *alternate access model* [Fig. 8(B)]. It is, therefore, an interesting question if the inversion of active transport can be induced in the system described by the *alternate access model* through the slowing down the conformational transitions. However, the pathway corresponding to the latter model is asymmetric with respect to the exchange of subsystems I and II. Therefore it is less likely to be a dominant pathway in our present model. We have presented a basic model here, but taken into the account of the effect of the asymmetry of subsystems or other features, our model will be more generic and gain a great variety of complex functions.

In summary, we have presented a simple model containing two ratchet subsystems coupled via an allosteric degree of freedom. The model can achieve the coupling of the fluxes conveyed by the subsystems. We found the inversion of active transport flux by the change of the time constant of the allosteric transition. The optimization of the rate constants to achieve high coupling ratio leads to a similar scheme to the actual transport protein. Model was also discussed from the regulatory point of view. We suggest that the coupled fluctuation of the subsystems (subunits or domains) through allosteric interaction is the origin of the diverse functions of the protein machineries.

[1] H. V. Westerhoff and Y. Chen, Proc. Natl. Acad. Sci. U.S.A. **82**, 3222 (1985).

[2] R. D. Astumian, P. B. Chock, T. Y. Tsong, and H. V. Westerhoff, Phys. Rev. A **39**, 6416 (1989).

[3] A. Ajdari and J. Prost, C. R. Acad. Sci., Ser. II: Mec., Phys., Chim., Sci. Terre Univers **315**, 1635 (1992).

[4] J. Prost, J.-F. Chauwin, L. Peliti, and A. Ajdari, Phys. Rev. Lett. **72**, 2652 (1994).

[5] M. O. Magnasco, Phys. Rev. Lett. **71**, 1477 (1993).

[6] M. O. Magnasco, Phys. Rev. Lett. **72**, 2656 (1994).

[7] R. D. Astumian and M. Bier, Biophys. J. **70**, 637 (1996).

[8] R. D. Astumian and M. Bier, Phys. Rev. Lett. **72**, 1766 (1994).

[9] T. D. Xie, Y. Chen, P. Marszalek, and T. Y. Tsong, Biophys. J. **72**, 2496 (1997).

[10] Y. A. Makhnovskii, V. M. Rozenbaum, D. Y. Yang, S. H. Lin, and T. Y. Tsong, Phys. Rev. E **69**, 021102 (2004).

[11] T. D. Xie, P. Marszalek, Y.-d. Chen, and T. Y. Tsong, Biophys. J. **67**, 1247 (1994).

[12] D. Nawarathna, J. H. Miller, Jr., J. R. Claycomb, G. Cardenas, and D. Warmflash, Phys. Rev. Lett. **95**, 158103 (2005).

[13] R. D. Astumian, Phys. Rev. Lett. **91**, 118102 (2003).

[14] O. Hod and E. Rabani, Proc. Natl. Acad. Sci. U.S.A. **100**,

14661 (2003).

[15] E. Muneyuki and T. A. Fukami, Biophys. J. **78**, 1166 (2000).

[16] E. Muneyuki, M. Ikematsu, and M. Yoshida, J. Phys. Chem. **100**, 19687 (1996).

[17] R. Kanada and K. Sasaki, Phys. Rev. E **67**, 061917 (2003).

[18] C. J. Brokaw, Biophys. J. **81**, 1333 (2001).

[19] R. D. Vale and F. Oosawa, Adv. Biophys. **26**, 97 (1990).

[20] O. Jardetzky, Nature (London) **211**, 969 (1966).

[21] J. Abramson, I. Smirnova, V. Kasho, Gillian Verner, H. Ronald Kaback, and So Iwata, Science **301**, 610 (2003).

[22] K. Sekimoto, Physica D **205**, 242 (2005).

[23] D. E. J. Koshland, G. Nemethy, and D. Filmer, Biochemistry **5**, 365 (1966).

[24] T. L. Hill, *Free Energy Transduction and Biochemical Cycle Kinetics* (Springer Verlag, New York, 1989).

[25] P. G. Bergmann and J. L. Lebowitz, Phys. Rev. **99**, 578 (1955).

[26] J. L. Lebowitz and P. G. Bergmann, Ann. Phys. **1**, 1 (1957).

[27] R. Dabrowska, A. Goch, H. Osinska, A. Szpacenko, and J. Sosinski, J. Muscle Res. Cell Motil. **6**, 29 (1985).

[28] N. Schrantz, M. T. Auffredou, M. F. Bourgeade, L. Besnault, G. Leca, and A. Vazquez, Cell Death Differ. **8**, 152 (2001).

[29] Y. Hashida and K. Inouye, J Biochem. (Tokoyo) **141**, 843 (2007).

[30] T. S. Komatsu and N. Nakagawa, Phys. Rev. E **73**, 065107(R) (2006).

[31] H.-X. Zhou and Y. D. Chen, Phys. Rev. Lett. **77**, 194 (1996).

[32] A. Parmeggiani, F. Julicher, A. Ajdari, and J. Prost, Phys. Rev. E **60**, 2127 (1999).

[33] P. D. Boyer, FEBS Lett. **58**, 1 (1975).